PAPER • OPEN ACCESS

On the sign of the linear magnetoelectric coefficient in Cr_2O_3

View the article online for updates and enhancements.

You may also like

On the sign of the linear magnetoelectric coefficient in Cr$_2$O$_3$*

Eric Bousquet[1], **Eddy Lelièvre-Berna**[2], **Navid Qureshi**[2], **Jian-Rui Soh**[3],
Nicola A Spaldin[4], **Andrea Urru**[4,5], **Xanthe H Verbeek**[4,**] and **Sophie F Weber**[4]

[1] University of Liège, Quartier Agora, Allée du Six Août 19, 4000 Liège 1, Belgium
[2] Institut Laue Langevin, 71 Avenue des Martyrs, CS 20156, 38042 Grenoble, France
[3] Laboratory for Quantum Magnetism, Institute of Physics, École Polytechnique Fédérale de Lausanne, CH-1015 Lausanne, Switzerland
[4] Materials Theory, ETH Zurich, Wolfgang-Pauli-Strasse 27, 8093 Zurich, Switzerland
[5] International School for Advanced Studies (SISSA), Via Bonomea 265, 34136 Trieste, Italy

E-mail: xverbeek@ethz.ch

CrossMark

Abstract

We establish the sign of the linear magnetoelectric (ME) coefficient, α, in chromia, Cr$_2$O$_3$. Cr$_2$O$_3$ is the prototypical linear ME material, in which an electric (magnetic) field induces a linearly proportional magnetization (polarization), and a single magnetic domain can be selected by annealing in combined magnetic (**H**) and electric (**E**) fields. Opposite antiferromagnetic (AFM) domains have opposite ME responses, and which AFM domain corresponds to which sign of response has previously been unclear. We use density functional theory (DFT) to calculate the magnetic response of a single AFM domain of Cr$_2$O$_3$ to an applied in-plane electric field at zero kelvin. We find that the domain with nearest neighbor magnetic moments oriented away from (towards) each other has a negative (positive) in-plane ME coefficient, $\alpha_\perp$, at zero kelvin. We show that this sign is consistent with all other DFT calculations in the literature that specified the domain orientation, independent of the choice of DFT code or functional, the method used to apply the field, and whether the direct (magnetic field) or inverse (electric field) ME response was calculated. Next, we reanalyze our previously published spherical neutron polarimetry data to determine the AFM domain produced by annealing in combined **E** and **H** fields oriented along the crystallographic symmetry axis at room temperature. We find that the AFM domain with nearest-neighbor magnetic moments oriented away from (towards) each other is produced by annealing in (anti-)parallel **E** and **H** fields, corresponding to a positive (negative) axial ME coefficient, $\alpha_\parallel$, at room temperature. Since $\alpha_\perp$ at zero kelvin and $\alpha_\parallel$ at room temperature are known to be of opposite sign, our computational and experimental results are consistent.

Keywords: magnetoelectric, neutron polarimetry, Cr$_2$O$_3$, antiferromagnets, density functional theory, antiferromagnetic domains

---

* Author names in alphabetical order, see author contribution statement.
** Author to whom any correspondence should be addressed.

1. Introduction

Materials in which both time-reversal Θ and space-inversion $\mathcal{I}$ symmetries are broken, while the product $\mathcal{I}\Theta$ symmetry is preserved, have a term in their free energy of the form

$$F(\mathbf{E},\mathbf{H}) = -\frac{1}{V}\alpha_{ij}E_i H_j, \tag{1}$$

where $\mathbf{E}/\mathbf{H}$ are electric/magnetic fields, α is the nine-component *magnetoelectric* tensor (SI units $\mathrm{s\,m^{-1}}$) and V is the unit cell volume. This term reveals two distinctive and related material properties. First, there is a preferred magnetic domain orientation, determined by the sign and form of α, in simultaneous magnetic and electric fields, so that annealing in such a combination of fields, called *magnetoelectric annealing*, can be used to select for a specific magnetic domain. Second, by differentiating equation (1) with respect to electric (magnetic) field to obtain the polarization (magnetization), we see that

$$P_i(\mathbf{E},\mathbf{H}) = -\frac{\partial F}{\partial E_i} = \frac{1}{V}\alpha_{ij}H_j, \tag{2}$$

and

$$M_i(\mathbf{E},\mathbf{H}) = -\frac{1}{\mu_0}\frac{\partial F}{\partial H_i} = \frac{1}{\mu_0 V}\alpha_{ji}E_i, \tag{3}$$

where μ_0 is the vacuum permeability. Equations (2) and (3) reveal a linear proportionality between an applied electric (magnetic) field and an induced magnetization M_i (polarization P_i), with α the response tensor. Materials with non-zero α therefore show a linear magnetoelectric (ME) effect and are promising for spintronic applications since they enable voltage-control of magnetism [1].

Corundum-structure chromia, Cr_2O_3, is the prototypical linear ME, and the first material in which the linear ME effect was predicted [2] and measured [3, 4]. In addition to its historical relevance, Cr_2O_3 has a high Néel temperature compared to other ME materials, and continues to be the primary material of focus in theoretical, experimental and technological studies of the ME effect. We show the primitive rhombohedral unit cell of Cr_2O_3 in figure 1(a). Below its Néel temperature T_N = 307 K [5], Cr_2O_3 adopts a superexchange-mediated easy-axis antiferromagnetic (AFM) 'up-down-up-down' ordering of the magnetic dipole moments on the d^3 Cr^{3+} ions along the rhombohedral $\langle 111 \rangle$ direction [6, 7]. The R3$'$c$'$ magnetic space group breaks both $\mathcal{I}$ and Θ while preserving $\mathcal{I}\Theta$, thus allowing a linear ME response [8]. In figure 1(b) we show the primitive unit cell of the opposite AFM domain, with 'down-up-down-up' magnetic dipole ordering. While (a) and (b) are energetically degenerate in the absence of external fields, they correspond to opposite ME domains. As a result, the signs of their linear ME responses are opposite, and they are obtained by ME annealing in opposite combinations of $\mathbf{E}$ and $\mathbf{H}$ fields. In figure 1(c), we show the unit cell of Cr_2O_3 in the hexagonal setting conventionally used in neutron diffraction, in which the hexagonal $\langle 001 \rangle$ axis is parallel to the rhombohedral $\langle 111 \rangle$ axis.
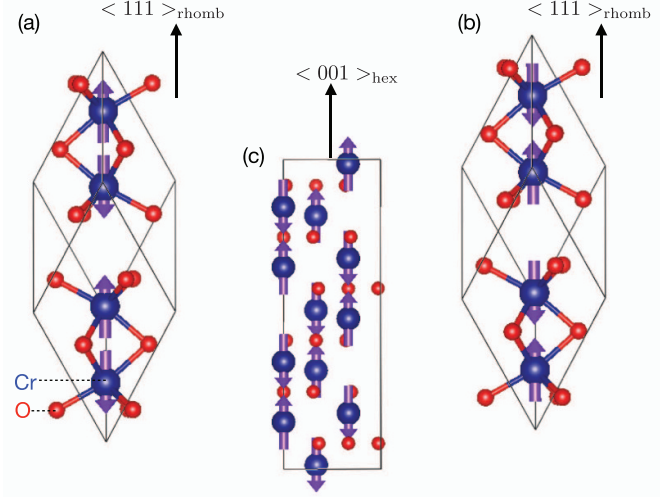

Figure 1. The crystal structure of Cr_2O_3 showing the primitive rhombohedral unit cell, with the two AFM domains, the 'out-pointing' domain (a) and the 'in-pointing' domain (b). The goal of this work is to determine the absolute signs of the components of α for the two individual domains. The hexagonal setting, which we use in our experimental discussion, is shown in (c) for the in-pointing magnetic domain. Note that $\langle 001 \rangle_{\mathrm{hex}} \parallel \langle 111 \rangle_{\mathrm{rhomb}}$.

The symmetry of the R3$'$c$'$ magnetic space group allows for a diagonal response tensor α, described by two independent components which we denote as $\alpha_\parallel$ and $\alpha_\perp$ [2]:

$$\begin{pmatrix} \alpha_\perp & 0 & 0 \\ 0 & \alpha_\perp & 0 \\ 0 & 0 & \alpha_\parallel \end{pmatrix}. \tag{4}$$

$\alpha_\parallel$ describes the magnetization (polarization) induced when $\mathbf{E}$ ($\mathbf{H}$) is applied along the rhombohedral $\langle 111 \rangle$ axis, and $\alpha_\perp$ refers to the perpendicular ME response when the field and induced property lie in the basal plane. Figure 2 shows the measured temperature dependence of $\alpha_\parallel$ and $\alpha_\perp$, extracted from the original experimental report [4]. While $\alpha_\perp$, which results from the $\mathbf{E}$-field induced canting of the magnetic dipole moments away from the easy axis [9, 10], follows the usual order-parameter onset below T_N, $\alpha_\parallel$ has a peak in magnitude just below T_N before decreasing and switching sign at low temperature. This is understood in terms of the response of spin fluctuations at high temperature [11], with the orbital magnetization response [10] dominating at low temperature. Importantly, at $T = 0$ K, relevant to first-principles calculations, $\alpha_\perp$ and $\alpha_\parallel$ have the same sign, whereas at room temperature, relevant to many experimental setups, $\alpha_\perp$ and $\alpha_\parallel$ have opposite signs.

While the *relative* signs of $\alpha_\perp$ and $\alpha_\parallel$ were established unambiguously in [3], it was not possible at the time to determine which set of α values correspond to the out-pointing or in-pointing magnetic domains of figures 1(a) and (b). Instead, [3] showed that reversal of the AFM domain reverses the signs of α as required by symmetry, and that the measured magnitudes in multi-domain or poly-crystalline samples are
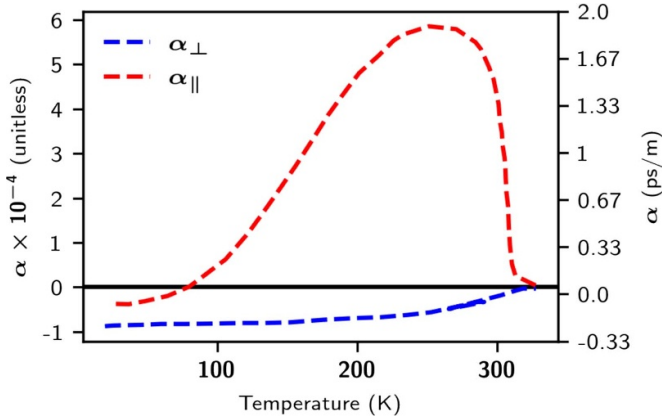
Figure 2. Temperature dependence of the parallel $\alpha_\parallel$ and perpendicular $\alpha_\perp$ ME responses in Cr_2O_3, extracted from [4]. α is given in dimensionless units (by multiplying by the speed of light) multiplied by 10^{-4} (left-hand *y* axis) and SI $ps\,m^{-1}$ units (right-hand *y* axis). Reproduced from [4], with permission from Springer Nature.

substantially reduced due to cancellation effects. The experimental determination of the specific bulk AFM domain corresponding to a particular ME response is highly non-trivial and requires a generalized form of polarized neutron scattering called spherical neutron polarimetry (SNP); to our knowledge only four such experiment has been performed for Cr_2O_3 [12–14]. While in principle first-principles calculations based on density functional theory (DFT) yield this information directly, the AFM domain modeled is often not reported in the literature, and the sensitivity of the magnetic anisotropy to the details of the DFT parameters render an independent experimental determination desirable. To compound confusion, in both the theoretical and experimental literature the terms 'magnetic moments' and 'spins' have sometimes been used interchangeably, in spite of their being opposite in sign.

The purpose of this paper is to establish unambiguously the signs of the ME effect corresponding to each of the two opposite AFM domains in Cr_2O_3. We achieve this goal by reviewing and reanalyzing the relevant computational and experimental literature, as well as presenting the results of our own new DFT calculations. In section 2, we begin by reviewing the DFT-based results for the zero-kelvin values of $\alpha_\perp$ and $\alpha_\parallel$, computed both by us and by others in earlier publications. We then perform a comprehensive cross-check of the domain-dependent sign of α using four different codes, three different methods for applying the external fields, and different choices of DFT parameters.

We find that the *ab-initio* results give consistent signs for α across authors, DFT parameters, and codes used.

In section 3, we reanalyze the seminal neutron polarimetry experiments which provided the first experimental indicator for the sign of α [12–15]. While the stated conclusion of the original polarimetry papers contradicts the DFT findings, we show that this is actually due to the assumed sample orientation with respect to the instrument axes during analysis in [13–15]. When we account for and correct these inconsistencies,

the raw polarimetry data indicate a room-temperature sign of α for a given AFM domain consistent with all DFT calculations (taking into account the experimental temperature dependence of α found by Astrov in figure 2). We hope that this paper clears up long-standing ambiguities and confusions in the literature, and facilitates future interpretations of theoretical and experimental data related to the ME effect in Cr_2O_3 and other ME materials.

2. Computational studies

Several *ab initio* studies of the magnitude and sign of the ME effect in Cr_2O_3 have been performed previously [9–11, 16, 17]. Three main techniques have been employed: Explicit inclusion of i) a static magnetic field or ii) a static electric field within the DFT Hamiltonian, and iii) the so-called 'lattice-mediated' method, in which a polar displacement of the ions simulates the application of an electric field. Both spin and orbital contributions to the response have been calculated, and α has been resolved into so-called *clamped-ion* (the electronic response to an electric field with fixed ions) and *lattice-mediated* (in which the ions are displaced by the electric field) components. Since most DFT codes (in particular ABINIT [18, 19], ELK [20], QUANTUM ESPRESSO [21, 22] and VASP [23, 24]) output magnetic moments rather than spins, we adopt this convention here.

First, we summarize the results of the various literature studies that report both the AFM domain studied and the sign of the calculated α. The technical details for each calculation are summarized in table 1. First, Malashevich *et al* [10] found $\alpha_\parallel$ and $\alpha_\perp$ to have the same positive sign at 0 K for a domain with in-pointing moments (as in figure 1(b)). They used the finite electric-field method so that both spin and orbital contributions and the full lattice-mediated and electronic responses were included. For the same domain, Íñiguez [9] used the 'lattice-mediated' method and obtained a positive 0 K lattice-mediated spin ME response $\alpha_\perp$; since [9] did not include orbital contributions, $\alpha_\parallel$ was zero. Also using the lattice-mediated approach but including the orbital contributions, Ye and Vanderbilt [16] found positive $\alpha_\parallel$ and $\alpha_\perp$ for the domain with in-pointing moments at 0 K. Bousquet *et al* [17], using an explicitly applied magnetic Zeeman field, including both the lattice-mediated and clamped-ion spin contributions, find a positive 0 K $\alpha_\perp$ for the in-pointing domain as well [26]. Finally, Mostovoy *et al* [11] considered the opposite domain (note that figure 1 of [11] shows *spins*) and calculated the finite-temperature spin contribution to $\alpha_\parallel$, using Monte-Carlo simulations of a DFT-derived model Hamiltonian containing Heisenberg exchanges and a magnetic moment—polarization coupling. They found a positive $\alpha_\parallel$ in the temperature range of $T = 60–400$ K, consistent with a negative $\alpha_\parallel$ at $T = 0$ K (figure 2). Since their calculations modeled the out-pointing domain, these results are consistent with the other computational studies discussed earlier.

To supplement the literature results, we perform a comprehensive cross-check of the domain-dependent sign of $\alpha_\perp$

Table 1. Overview of parameters used in different DFT calculations, performed with different codes (QE stands for QUANTUM ESPRESSO). The short-hand notations for pseudopotentials (PP) and exchange-correlation functionals (XC) are: projected-augmented wave (PAW) [25], norm-conserving (NC), ultra-soft (US), all-electron (AE), local-density approximation (LDA) and generalized-gradient approximation with the Perdew–Burke–Ernzerhof (PBE) parametrization. SOC denotes spin–orbit coupling and the different contributions to α are indicated with LM (lattice-mediated) and CI (clamped-ion), spin (S) and orbital (O).

Source	Code	PP	XC	U (eV)	SOC	Unit cell	Contributions to α	Method	$\alpha_\perp$		$\alpha_\parallel$	
									ps m^{-1}	g.u. ($\times 10^{-4}$)	ps m^{-1}	g.u. ($\times 10^{-4}$)
[10]	QE	NC	PBE	No U	Yes	PBE	LM + CI, S + O	Electric field	−1.04	−3.12	−0.02	−0.06
[9]	VASP	PAW	LDA	$U_{\mathrm{eff}} = 2$	Yes	Expt.	LM, S	Lattice-mediated	−0.43	−1.3		
[16]	QE	NC	PBE	No U	Yes	PBE	LM, S + O	Lattice-mediated	−0.658	−1.97	−0.0221	−0.0663
[17]	VASP	PAW	LDA	$U_{\mathrm{eff}} = 2$	Yes	Expt.	LM + CI,S	Zeeman field	−1.45	−4.35		
[11][a]	VASP	PAW	LDA	$U_{\mathrm{eff}} = 2$	No	Expt.	LM + CI, S	Magnetic exchange			3.77	11.3
This work	ELK	AE	LDA	U = 4.0 J = 0.5	Yes	LDA	LM, S	Lattice-mediated	−0.921	−2.76		
This work	VASP	PAW	LDA	U = 4.0 J = 0.5	Yes	LDA	LM, S	Lattice-mediated	−0.857	−2.57		
This work	QE	US	PBE	No U	Yes	PBE	LM, S	Lattice-mediated	−0.773	−2.32		
This work	Abinit	NC	LDA	No U	Yes	Expt.	LM + CI, S	Zeeman field	−1.48	−4.44		
This work	Abinit	NC	LDA	No U	Yes	Expt.	LM + CI, S	Electric field	−1.48	−4.44		

[a] Results obtained at $T = 240$ K.

using four different codes and three different methods [27]. First, we calculate the lattice-mediated spin contribution to $\alpha_\perp$ using the lattice-mediated method, as described in [9], using the ELK [20], VASP [23, 24], and QUANTUM ESPRESSO [21, 22] codes, with the parameters listed in table 1. In all cases we find $\alpha_\perp < 0$ for the out-pointing domain at 0 K, consistent with the literature findings summarized above. In addition, we use the ABINIT code [18, 19] to calculate the spin contribution to the ME effect by both explicitly applying an electric field as in [10], and a magnetic Zeeman field method as in [17]. Both methods give the same positive value of $\alpha_\perp$ for the in-pointing domain at 0 K. Computational details for the calculations in ELK, VASP, QUANTUM ESPRESSO, and ABINIT can be found in appendices A–D. We list our calculated $\alpha_\perp$ values in table 1, and in figure 3, we plot the induced in-plane magnetizations as a function of in-plane electric fields calculated here and from the literature. Although there is complete agreement on the sign of α, it is clear that there is some spread in the magnitude of calculated values. This distribution cannot be explained only by the different contributions to α that were taken into account, and is most likely also the result of the different choices in electronic structure code, electronic exchange parameters and convergence criteria. Considering these differences, the agreement on the magnitude of α is remarkable.

In summary, the calculated signs of α are consistent across DFT codes and methodologies, with the 0 K $\alpha_\perp$ and $\alpha_\parallel$ positive for the in-pointing domain, the 0 K $\alpha_\perp$ negative for the out-pointing domain, and the room temperature $\alpha_\parallel$ positive for the out-pointing domain. We summarize this result in table 2, where we also inferred the sign of $\alpha_\parallel$ for the in-pointing domain at room temperature from the knowledge that it must be opposite to the sign of $\alpha_\parallel$ for the out-pointing domain at room temperature. Similarly, we infer the sign of $\alpha_\parallel$ for the out-pointing domain at 0 K. Finally, the signs of $\alpha_\perp$ at room
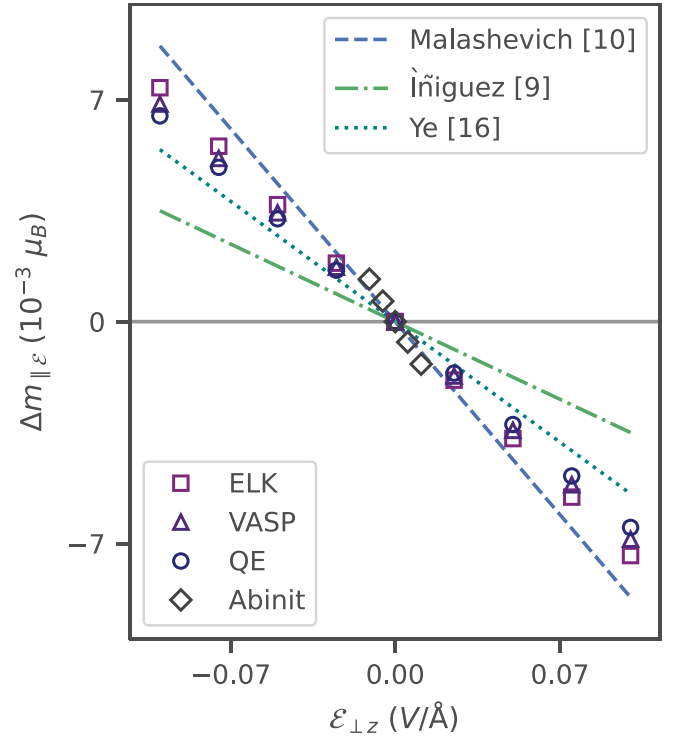

Figure 3. Induced net magnetic moment per rhombohedral unit cell parallel to an applied electric field oriented perpendicular to the easy axis, as a function of electric field strength for the out-pointing domain. The three lines show the response calculated from literature $\alpha_\perp$ values. Markers indicate our results using four different DFT codes.

temperature are inferred from the sign at 0 K and the knowledge from experiment (figure 2) that $\alpha_\perp$ maintains the same sign at 0 K and room temperature.

Table 2. The sign of alpha for the two domains, at 0 K and room temperature (RT) as determined by different *ab initio* calculations. Note that not always both domains were calculated explicitly, but we infer the sign of α in one domain from the sign of α in the other, as they have to be opposite. Thus, we infer the sign of $\alpha_\parallel$ for the out-pointing domain at 0 K and for the in-pointing domain at RT. $\alpha_\perp$ at RT was not calculated, but is inferred from the 0 K results, as it is known not to change sign between 0 K and RT, from the temperature dependence measured by Astrov, see figure 2. The inferred signs are displayed in grey, while the explicitly calculated ones are in black and bold.

		$\alpha_\parallel$	$\alpha_\perp$
0 K	Out-pointing domain	−	**−**
	In-pointing domain	**+**	**+**
		$\alpha_\parallel$	$\alpha_\perp$
RT	Out-pointing domain	**+**	−
	In-pointing domain	−	+

3. Experimental studies

To our knowledge, there exist four sets of data in which the magnetic structure of Cr_2O_3 was measured using SNP, the generalized form of polarized neutron scattering [12–15]. This technique allows for both the detection of the domain imbalance between the two different magnetic structures shown in figure 1, and for the determination of the magnetic moment configuration of the predominant domain [12]. This is possible because with SNP, the polarization vectors of both the incident and scattered neutron beams are determined; in comparison, in conventional (uniaxial) polarized neutron scattering, the scattered neutron polarization information is only analyzed along the direction of the incident beam polarization [28]. Therefore, SNP is an ideal method for elucidating which spin configuration shown in figure 1 is stabilized by the parallel or anti-parallel combination of electric and magnetic fields.

The SNP measurements reported in [12–15] were performed at the IN20 and D3 beamlines at the Institut Laue Langevin (ILL, Grenoble), using the CRYOgenic Polarization Analysis Device (Cyopad). The Cryopad consists of a zero-magnetic field sample chamber surrounded by magnetic fields manipulating the incident ($\mathbf{P}_i$) and scattered ($\mathbf{P}_f$) beam polarizations [29, 30]. The field regions are decoupled with a pair of concentric superconducting Meissner shields combined with μ-metal yokes and screens. The incident neutron beam polarization was controlled using a combination of a nutator and precession coil, and was oriented along one of three orthogonal experimental co-ordinates which were defined as x, which is along the direction of the scattering vector $\mathbf{Q}$, z, which is perpendicular to the horizontal scattering plane, and y, which completes the right-handed co-ordinate set. The polarization of the scattered neutron beam was also analyzed along these three principal axes using another set of precession and nutator coils.

In each of the four studies, the Cr_2O_3 sample was aligned so that the crystal b-axis was perpendicular to the horizontal

scattering plane, which allowed access to the $(h\,0\,l)$ reflections (importantly, this introduces an ambiguity between $b\|+z$ and $b\|-z$, which we will discuss in more detail in the following section). Here, the Miller indices correspond to the hexagonal setting of the rhombohedral ($R\bar{3}c$) unit cell of Cr_2O_3 adopted in [12–15]. In the three most recent studies, prior to installing the sample in the Cryopad for the SNP measurements, the Cr_2O_3 sample was cooled through the Néel temperature ($T_N \sim$ 310 K) in a combination of electric and magnetic fields oriented along the crystallographic c axis to achieve an imbalance of 180° domain population [12–14]. Brown *et al* reported that this annealing process stabilized a single AFM domain [12–14], and that the type of AFM domain (figure 1) could be chosen based on the relative orientation of the external magnetic ($\mathbf{H}$) and electric fields ($\mathbf{E}$). The experimental determination of which magnetic domain is favored then boils down to the determination and interpretation of the sign of the polarization matrix element P_{zx}.

Experimentally, P_{zx} is determined by measuring two quantities, namely n_{zx} and $n_{z\bar{x}}$, which are the number of scattered neutrons with the polarization parallel and antiparallel to $+x$ for the incident neutron polarization along $+z$. The experimental P_{zx} matrix element is in turn obtained by taking the ratio,

$$P_{zx} = \frac{n_{zx} - n_{z\bar{x}}}{n_{zx} + n_{z\bar{x}}}, \tag{5}$$

for a given Bragg reflection $\mathbf{Q} = (h\,k\,l)$. As such, the quantity P_{zx} is bounded between -1 and 1.

In order to determine which AFM domain is favored, the authors in [12–15] expressed P_{zx} in terms of three dimensionless quantities,

$$P_{zx} = \eta \frac{-2q_y\gamma}{1+\gamma^2}. \tag{6}$$

The η term defines the population imbalance between the two magnetic domains, and is given by $\eta = (v^+ - v^-)/(v^+ + v^-)$, where v^+ and v^- are the volumes of the two magnetic domains. Hence, the value of η is bounded between 1 and -1. If the two magnetic domains are equally populated, the factor η becomes 0. The term q_y is determined by the orientation of the crystal with respect to the experimental set up, with the sign of q_y depending on whether the crystallographic $+b$ axis is along the $+z$ or $-z$ direction of the experimental geometry; for example q_y is $+1$ (-1) if the magnetic interaction vector $\mathbf{M}_\perp(\mathbf{Q})$ is parallel (anti-parallel) to the $+y$ axis of the experimental geometry. Hence, it is crucial to determine whether $+b$ is along the $+z$ or $-z$ direction. Finally, the term γ is associated with the magnetic structure, with the sign of γ being positive (negative) for the out-pointing (in-pointing) magnetic domain.

Based on this discussion, we identify three inconsistencies across the four [12–15], which we clarify here. (Note that the measurements in [12–15] were made with the same crystal by the same group of coauthors so we expect the underlying physics to be consistent).

3.1. Spin vs magnetic moment

The first discrepancy is between [12, 14], regarding the definition of spin **S** and magnetic moments **μ**. In [14], Brown *et al* propose that the antiparallel **E** and **H** fields favor the 'out-pointing' arrows (figure 1(a)) and designate the arrows as spin directions. On the other hand in [12], Brown *et al* present 'in-pointing' arrows (figure 1(b)), which they designate as magnetic moments, and state that this magnetic structure is stabilized by parallel **E** and **H** fields. These two statements are incompatible, since the Cr spin direction and magnetic moment direction are anti-parallel, i.e. $\boldsymbol{\mu}_s = -g_s \mu_B \mathbf{S}/\hbar$, where g_s is the electron *g*-factor.

In the neutron scattering community, however, the terms spin and magnetic moment are often used interchangeably to mean magnetic moment direction. We should therefore assume that the arrows in [14] actually indicate magnetic moments, rather than spins as stated. This resolves the apparent discrepancy between [12, 14].

3.2. Orientation of the crystal b axis

Second, the labeling of the Miller indices $(h0l)$ across the four reports is inconsistent. In the first report [15], the two reported reflections, namely (102) and $(\bar{1}04)$, are in fact forbidden by the $R\bar{3}c$ space group in the hexagonal setting of Cr_2O_3. In the subsequent study, the two reported reflections, $(\bar{1}02)$ and $(10\bar{2})$ are both allowed by $R\bar{3}c$. In the following two reports [13, 14], where forty reflections were reported in total, thirty-two are in fact forbidden by the $R\bar{3}c$ space group of Cr_2O_3. The *h* and *l* Miller indices of the remaining eight reflections are both multiples of 3, e.g. (306) and $(30\bar{6})$, and are hence allowed.

Given that the magnetic propagation vector of Cr_2O_3 is $\mathbf{Q}_m = (000)$, the magnetic scattering intensity occurs at the same reciprocal space location as the structural Bragg peaks of Cr_2O_3. As such, the Miller index of the magnetic/nuclear reflections should follow the general condition of the $R\bar{3}c$ space group, where $-h+k+l = 3n$. Since the four reports were concerned with reflections in the $(h0l)$ plane, the observed reflections should obey the rule $-h+l = 3n$, given that $k = 0$. In figure 4(a) we plot the calculated reciprocal space maps for Cr_2O_3 in the $(h0l)$ scattering plane, assuming that the $+b$ crystal axis is along the $+z$ direction as stated in the original papers. Here, the allowed reflections, such as $(\bar{1}02)$ and (104), are denoted by the black filled circles, and the reciprocal space location of the forbidden reflections that do not obey $-h+l = 3n$ are shown by the crosses ($\times$).

The observed reflections in [13–15] are denoted by the arrows in the reciprocal space map. Indeed, many of the observed reflections, including (102) and $(10\bar{4})$, are in fact forbidden by the $R\bar{3}c$ space group.

If instead, we assume that the $+b$ crystal axis was oriented along the $-z$ direction (rather than $+z$), then the reciprocal space location of all forty-two observed reflections reported in [13–15], is fully compatible with the $R\bar{3}c$ space group. This scenario is very plausible, due to a possible mix up between the
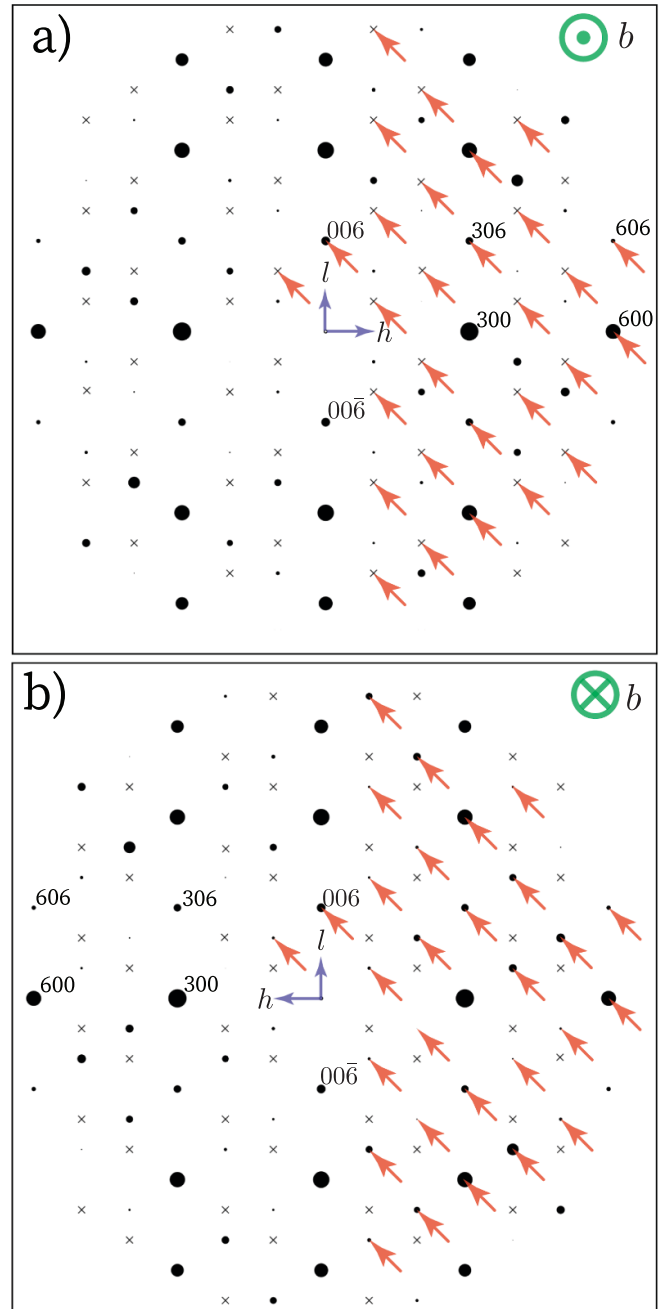

Figure 4. Plan view of the horizontal scattering plane of the reciprocal space map of Cr_2O_3, with the crystal *b* axis (a) along the $+z$ direction quoted in [13–15] and (b) $-z$ directions, respectively. Here the filled circles indicate the allowed reflections, with the size of the circle proportional to the neutron scattering cross-section, whereas the cross ($\times$) denotes forbidden reflections. (a), The arrows indicate the reciprocal space location of the observed reflections in [13–15], of which many are forbidden by the $R\bar{3}c$ space group of Cr_2O_3. (b), Instead, if the crystal *b* axis were actually along the $-z$ direction, then the observed reflections denoted by the arrows can be accounted for.

$+b$ and $-b$ crystal axes, which are inequivalent in Cr_2O_3. As shown in figure 4(b), where we plot the calculated reciprocal space maps for Cr_2O_3 in the $(h0l)$ scattering plane, assuming that the $+b$ crystal axis is along the $-z$ direction, the reciprocal

Table 3. Comparison between the measured ($P_f^{\text{obs.}}$) and calculated ($P_f^{\text{calc.}}$) polarization matrices with 'out-pointing' and 'in-pointing' magnetic domain for the data collected with **E** and **H** parallel. The data is consistent with the 'out-pointing' magnetic domain, as shown in figure 1(a).

| | | | | | Parallel **H** and **E** | | | | | | | | | | | |
| | | | | | P_i | | | $P_f^{\text{obs.}}$ | | | $P_f^{\text{calc.}}$ Out pointing | | | $P_f^{\text{calc.}}$ In pointing | | |
Crystal	(hkl)	Axis$\|z$	Axis$\|$**H**	Axis$\|$**E**	x	y	z	x	y	z	x	y	z	x	y	z
I	$\bar{1}02$	010	001	001	0.00	0.00	0.88	0.83	0.06	0.08	0.88	0.00	0.00	−0.88	0.00	0.00
		0$\bar{1}$0	00$\bar{1}$	00$\bar{1}$	0.00	0.00	0.72	−0.69	0.06	−0.06	−0.72	0.00	0.00	0.72	0.00	0.00
		0$\bar{1}$0	001	001	0.00	0.00	0.72	−0.70	0.05	−0.05	−0.72	0.00	0.00	0.72	0.00	0.00
II	$10\bar{2}$	0$\bar{1}$0	00$\bar{1}$	00$\bar{1}$	0.88	0.00	0.00	−0.10	0.00	0.86	0.00	0.00	0.88	0.00	0.00	−0.88
		0$\bar{1}$0	00$\bar{1}$	00$\bar{1}$	0.00	0.88	0.00	0.06	0.88	0.03	0.00	0.88	0.00	0.00	0.88	0.00
		0$\bar{1}$0	00$\bar{1}$	00$\bar{1}$	0.00	0.00	0.88	−0.87	0.03	0.02	−0.88	0.00	0.00	0.88	0.00	0.00

space location of the observed reflections denoted by all of the arrows can now be accounted for.

Changing the direction of the $+b$ axis has two main consequences for the interpretation of the results in [13–15]. First it swaps the h Miller index of the reflections, such that the observed peaks which were designated as $(h0l)$ should be assigned as $(\bar{h}0l)$ instead. This would allow the thirty-four reflection which are originally forbidden now be compatible with $R\bar{3}c$, i.e. to obey the $-h+l=3n$ condition. The remaining eight reflections which have the h and l Miller indices both being multiples of 3, still obey this condition. The second is that in [12] the sign of q_y changes, which means that the interpretation of which magnetic domain is favored also changes.

Therefore, we conclude that the conjugate field with **E** and **H** parallel favors the 'out-pointing' domain, as shown in figure 1(a). By the same token, the antiparallel **E** and **H** field favors the 'in-pointing' domain. This is opposite to the interpretation in [14].

3.3. Sign of γ

Finally, the third inconsistency is between [13, 14]. In these studies, the γ term was obtained by measuring the polarization P_{zx} component of various reflections. Brown *et al* [13] reports, in table 3, the γ values for twelve reflections obtained on the IN20 instrument with thermal neutrons ($\lambda = 1.532$ Å). On the other hand, [14] reports the measurements of γ for a further fifteen reflections acquired on the D3 instrument with hot neutrons. Table 2 of [14] lists the γ data acquired from the D3 instrument along with those measured on the IN20 instrument, which were reported in [13].

The discrepancy lies in the sign of γ of the data collected on the IN20 instrument, which are reported both in table 2 of [14] and also in table 3 of [13]. Although the Miller indices of the twelve reflections and their corresponding magnitude of γ are the same, the signs are different. Since the sign of γ is used to interpret whether the magnetic domain is 'out-pointing' or 'in-pointing', this discrepancy calls into question which sign of γ was measured.

To resolve the ambiguity, here we use the MAG2POL software [31] to re-analyze the measured spherical neutron polarimetry data presented in table 2 of [12]. We choose this data set because the Miller indices are allowed by the $R\bar{3}c$ space group, and the raw data are presented explicitly. Moreover, these measurements were performed on cooling the Cr_2O_3 sample with a conjugate field of parallel or anti-parallel **E** and **H** fields through T_N to $T = 290$ K, where the measurements were performed. Tables 3 and 4 tabulate the measured polarization matrices for the case where **E** and **H** are parallel and anti-parallel, respectively, along with the results of our new analysis for the two cases where the magnetic domain is 'out-pointing' or 'in-pointing'.

Our analysis assuming an 'out-pointing' domain is consistent with the measured scattered neutron polarization for the case where **E** and **H** are parallel, contrary to the conclusions in [12–15]. Similarly, for the case where **E** and **H** are anti-parallel, we find that the measured polarization matrices are consistent with an 'in-pointing' domain.

4. Conclusion

We have combined a literature review, new *ab-initio* results, and a careful reanalysis of spherical neutron polarimetry data in an effort to resolve long-standing confusion regarding the domain-dependent sign of the ME coefficient in Cr_2O_3. We have shown that all *ab-initio* results to date are in agreement in the assignments of negative and positive low-temperature α to the out-pointing and in-pointing domains depicted in figure 1. These conclusions are remarkably consistent across multiple codes and methods. Gratifyingly, the room-temperature spherical neutron polarimetry *data* are consistent with the low-temperature *ab-initio* findings given that the room-temperature sign of $\alpha_\|$ is opposite to its low-temperature sign. The opposite interpretation in some of our literature experimental papers stems from a sign error due to subtle inconsistencies in the analysis which we discussed in section 3. The confusion and deceptive inconsistency have also been compounded in the past by ambiguous terminology from numerous authors

Table 4. Comparison between the measured ($P_f^{\mathrm{obs.}}$) and calculated ($P_f^{\mathrm{calc.}}$) polarization matrices with 'out-pointing' and 'in-pointing' magnetic domain for the data collected with **E** and **H** anti-parallel. The data is consistent with the 'in-pointing' magnetic domain, as shown in figure 1(b).

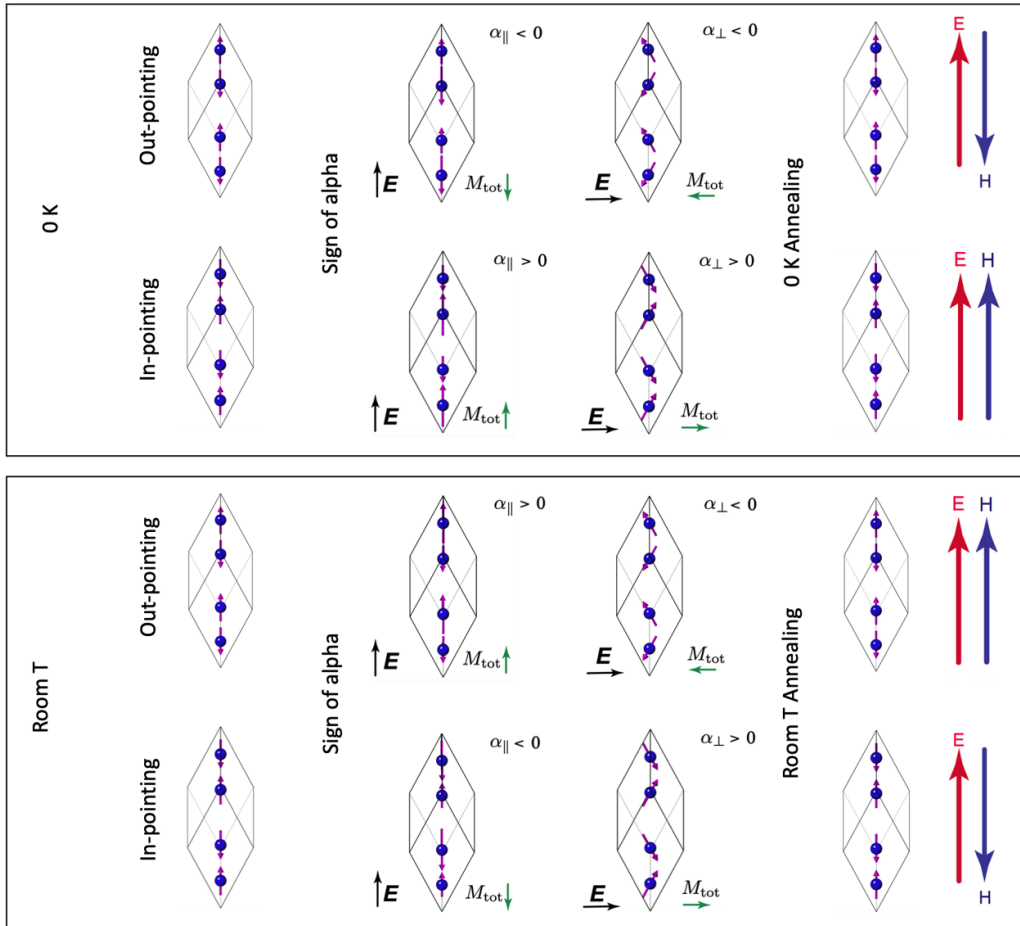| | | | | | | | | | | | | | | $P_f^{\mathrm{calc.}}$ | | | $P_f^{\mathrm{calc.}}$ | |
| | | | | | | | | | | | | | Out pointing | | | In pointing | | |
Crystal	(hkl)	Axis$\|z$	Axis$\|$**H**	Axis$\|$**E**	x	y	z	x	y	z	x	y	z	x	y	z
I	$\bar{1}02$	$0\bar{1}0$	001	$00\bar{1}$	0.00	0.00	0.72	0.71	0.12	0.02	−0.72	0.00	0.00	0.72	0.00	0.00
		$0\bar{1}0$	$00\bar{1}$	001	0.00	0.00	0.72	0.70	0.16	0.05	−0.72	0.00	0.00	0.72	0.00	0.00
II	$10\bar{2}$	$0\bar{1}0$	$00\bar{1}$	001	0.88	0.00	0.00	0.12	0.00	−0.85	0.00	0.00	0.88	0.00	0.00	−0.88
		$0\bar{1}0$	$00\bar{1}$	001	0.00	0.88	0.00	0.00	0.88	−0.05	0.00	0.88	0.00	0.00	0.88	0.00
		$0\bar{1}0$	$00\bar{1}$	001	0.00	0.00	0.88	0.86	0.12	0.14	−0.88	0.00	0.00	0.88	0.00	0.00
II	$\bar{1}02$	$0\bar{1}0$	$00\bar{1}$	001	0.88	0.00	0.00	0.10	0.06	−0.86	0.00	0.00	0.88	0.00	0.00	−0.88
		$0\bar{1}0$	$00\bar{1}$	001	0.00	0.88	0.00	−0.09	0.88	0.02	0.00	0.88	0.00	0.00	0.88	0.00
		$0\bar{1}0$	$00\bar{1}$	001	0.00	0.00	0.88	0.87	0.03	0.08	−0.88	0.00	0.00	0.88	0.00	0.00

*Header note: the "Anti-parallel **H** and **E**" spanning label and the P_i and $P_f^{\mathrm{obs.}}$ column groups appear above the x, y, z sub-columns for P_i and $P_f^{\mathrm{obs.}}$ respectively.*

Figure 5. The in- and out-pointing domains of Cr$_2$O$_3$ with the sign of $\alpha_\perp$ and $\alpha_\|$ and alignment of the **E** and **H** fields during the ME annealing that favors each domain at 0 K and at room temperature.

related to the usage of 'spin' versus 'magnetic' moment. We summarize the relationship between the domains and the sign of α, as well as the necessary alignment of the **E** and **H** fields during ME annealing, in figure 5.

We mention here an important consequence of our work for a related feature of Cr$_2$O$_3$; the magnitude and sign of the uncompensated magnetization on the (001) surface for a given bulk domain [32, 33]. At the 0-K limit in the absence of

thermal fluctuations, the direction of the (001) surface magnetization is unambiguously determined by the bulk domain which is selected in the ME annealing process. For example, with the in-pointing domain depicted for the hexagonal cell in figure 1(c), the surface magnetization from the dangling Cr at the (001) surface points outwards (positive). However, for any experimental characterizations performed at room-temperature, the relation between the bulk domain and the sign of surface magnetization is much less clear. Indeed, recent DFT-Monte Carlo calculations performed by Weber and Spaldin [34] indicate that the (001) surface magnetic moments of Cr_2O_3 are essentially paramagnetic at room temperature due to weak coupling to the bulk order parameter. Thus, it is likely that for a fixed domain, the surface magnetization is substantially reduced, or even switches sign, with respect to its 0 K value. Now that we have definitively determined which domain is selected by a given ME annealing at room temperature, it will be very interesting to re-examine, and perform new, experimental measurements of surface magnetization to determine its sign for an unambiguous selection of bulk domain.

We hope that our work convincingly demonstrates the previously questioned consistency of computational and experimental findings on the sign of the ME coefficient in Cr_2O_3, and that it may motivate new, updated polarimetry measurements to test and confirm existing experimental and theoretical results. We also hope that this paper will assist in the correct interpretation of future studies of Cr_2O_3, as well as providing a cautionary tale for similar investigations of other ME materials.

Data availability statement

All data that support the findings of this study are included within the article (and any supplementary files).

Acknowledgments

Author contributions

X H V performed the calculations in ELK and VASP, A U performed those in Quantum ESPRESSO and E B those in ABINIT. J R S, N Q and E L B performed the re-analysis of the SNP data. N A S conceived of and coordinated the project. All authors co-wrote the manuscript.

Conflict of interest

The authors declare that there is no conflict of interest.

Appendix A. Computational details ELK

Our DFT calculations in the augmented-plane wave (APW) code ELK were performed with spin–orbit interaction included, using the non-collinear local spin density approximation (LSDA) [35]. Correlation effects were taken into account by applying a rotationally invariant Hubbard U correction [36] on the Cr d states, with U = 4.0 eV and J = 0.5 eV, which well describe the physics of Cr_2O_3 [8, 37, 38]. Muffin-tin spheres were used to describe the Cr and O core states, with radii of 1.0716 Å and 0.804 35 Å. These radii are reduced by 4% with respect to the standard setting to prevent overlap of the muffin-tin spheres. The APW functions and the potential were expanded in a spherical harmonics basis, with cut-offs $l_{max(apw)} = l_{max(o)} = 12$. A $6 \times 6 \times 6$ Γ-centered k-point mesh was used to sample the Brillouin zone (BZ) [39]. We obtained the spin contributions to the lattice-mediated ME response in the xy-plane using the lattice-mediated method of [9], in which the response is constructed from a superposition of the magnetic moments induced by freezing in those eigenmodes of the force constant matrix that give a net polarization, in this case those with E_u symmetry. We used LSDA + U relaxed lattice parameters and atomic positions obtained from VASP calculations (see the description below). Force constant matrix eigenmodes and their energies were obtained from VASP interfaced with phonopy [40, 41]. Born effective charges, used to calculate the polarization, were taken from VASP calculations as well.

Appendix B. Computational details VASP

In the plane-wave code VASP, we performed DFT calculations with the LSDA+U method, spin–orbit coupling included, and a Hubbard U correction on the Cr d states, with U (J) = 4.0 (0.5) eV, as in the ELK calculations. The ionic cores of Cr and O were described with projector-augmented wave pseudopotentials [25]. We used the following settings for the valence electrons: Cr $3p^6 3d^5 4s^1$ and O $2s^2 2p^4$, corresponding to the datasets Cr_sv and O. We used a kinetic energy cut-off of 800 eV for the wavefunctions and performed the BZ integrations using a uniform Γ-centered $7 \times 7 \times 7$ k-point mesh. Structural and electronic relaxations performed with these parameters yielded a band gap and magnetic moment

close to known experimental values and lattice parameters of $a = 5.31$ Å, the length of the rhombohedral unit cell vectors and $\alpha = 54.87°$, the angle between the unit cell vectors. These values are 0.78% and 0.26% smaller than experiment [42]. As for the ELK calculations, we used the method of [9] to construct the lattice-mediated spin response to an applied electric field, from the net spin magnetic moment induced by freezing in appropriate eigenmodes of the force constant matrix. The eigenmodes and corresponding energies were calculated by interfacing VASP with phonopy. The polarizations of each of the eigenmodes were obtained from the product of the atomic displacements of the mode and the Born effective charges Z^e. We computed the Z^e by displacing each atom in the unit cell along each Cartesian direction and determining the ionic polarization using the modern theory of polarization, as implemented in VASP in the LCALCPOL routine. These calculations were performed for four displacements of different magnitudes, allowing us to assess the linear response regime. The final Z^e were obtained from the average of the Z^e for different atoms of the same species and different displacements within the linear regime.

Appendix C. Computational details Quantum Espresso

First-principles calculations in `Quantum ESPRESSO` [21, 22] and `thermo_pw` [43] were performed in non-collinear DFT using the generalized gradient approximation, with the Perdew–Burke–Ernzerhof parametrization of the exchange-correlation energy [44]. Ions were described by fully relativistic ultrasoft pseudopotentials (PPs) [45], with $3s$, $3p$, $4s$, and $4d$ valence electrons for Cr (PP `Cr.rel-pbe-spn-rrkjus_psl.0.2.3.UPF` from pslibrary 1.0.0 [46, 47]) and with $2s$ and $2p$ valence electrons for O (PP `O.rel-pbe-n-rrkjus_psl.0.1.UPF` from pslibrary 0.1). The pseudo wavefunctions (charge density) were expanded in a plane-wave basis set with kinetic energy cut-off of 140 (560) Ry. BZ integrations were performed using a shifted **k**-points mesh of $6 \times 6 \times 6$ points. The lattice-mediated spin contribution to the ME response was computed following the approach of [9]: specifically, Born effective charges and phonon frequencies at Γ were computed using density functional perturbation theory [48].

Appendix D. Computational details Abinit

The ABINIT calculations (version 8.8) were done with the norm-conserving pseudo-potentials coming from the PseudoDojo project [49] (v0.3) and within the LDA approximation for the exchange correlation functional without Hubbard U correction. We used a kinetic energy cut-off of 40 Ha (1088 eV) for the plane-wave expansion and integrated the BZ using a Monkhorst–Pack **k**-points mesh of $3 \times 3 \times 3$ points, shifted by (0.5, 0.5, 0,5). Spin–orbit coupling was included in all the calculations for both applied Zeeman field and applied electric field calculations. The cell parameters and shape were fixed to the experimental ones ($a = 5.37$ Å and

$\alpha = 55.13°$). The forces were relaxed up to a tolerance of 2.7×10^{-8} eV Å^{-1} and the SCF cycles to a tolerance of 2.7×10^{-9} eV Å^{-1} on the force residual.

ORCID iDs

Eric Bousquet https://orcid.org/0000-0002-9290-3463
Eddy Lelièvre-Berna https://orcid.org/0000-0002-6999-6489
Navid Qureshi https://orcid.org/0000-0002-0727-2258
Nicola A Spaldin https://orcid.org/0000-0003-0709-9499
Andrea Urru https://orcid.org/0000-0002-5602-3063
Xanthe H Verbeek https://orcid.org/0000-0003-2262-5047
Sophie F Weber https://orcid.org/0000-0001-6932-0377

References

[1] Borisov P, Hochstrat A, Shvartsman V V, Kleemann W and Hauck P M 2008 Magnetoelectric Cr_2O_3 for spintronic applications *Integr. Ferroelectr.* **99** 69–76
[2] Dzyaloshinskii I E 1960 On the magneto-electrical effect in antiferromagnets *Sov. Phys.-JETP* **10** 628–9
[3] Astrov D N 1960 The magnetoelectric effect in antiferromagnetics *Sov. Phys.-JETP* **11** 708–9
[4] Astrov D N 1961 Magnetoelectric effect in chromium oxide *Sov. Phys.-JETP* **13** 729
[5] Brockhouse B N 1953 Antiferromagnetic structure in Cr_2O_3 *J. Chem. Phys.* **21** 961–2
[6] Dudko K L, Eremenko V V and Semenenko L M 1971 Magnetostriction of antiferromagnetic Cr_2O_3 in strong magnetic fields *Phys. Status Solidi* b **43** 471–7
[7] Tobia D, De Biasi E, Granada M, Troiani H E, Zampieri G, Winkler E and Zysler R D 2010 Evolution of the magnetic anisotropy with particle size in antiferromagnetic Cr_2O_3 nanoparticles *J. Appl. Phys.* **108** 104303
[8] Fechner M, Sukhov A, Chotorlishvili L, Kenel C, Berakdar J and Spaldin N A 2018 Magnetophononics: ultrafast spin control through the lattice *Phys. Rev. Mater.* **2** 064401
[9] Iniguez J 2008 First-principles approach to lattice-mediated magnetoelectric effects *Phys. Rev. Lett.* **101** 117201
[10] Malashevich A, Coh S, Souza I and Vanderbilt D 2012 Full magnetoelectric response of Cr_2O_3 from first principles *Phys. Rev.* B **86** 094430
[11] Mostovoy M, Scaramucci A, Spaldin N A and Delaney K T 2010 Temperature-dependent magnetoelectric effect from first principles *Phys. Rev. Lett.* **105** 087202
[12] Brown P J, Forsyth J B and Tasset F 1998 A study of magnetoelectric domain formation in Cr_2O_3 *J. Phys.: Condens. Matter* **10** 663–72
[13] Brown P J, Forsyth J B and Tasset F 1999 Precision determination of antiferromagnetic form factors *Physica* B **237** 215–20
[14] Brown P J, Forsyth J B, Lelièvre-Berna E and Tasset F 2002 Determination of the magnetization distribution in Cr_2O_3 using spherical neutron polarimetry *J. Phys.: Condens. Matter* **14** 1957–66
[15] Tasset F, Brown P J and Forsyth J B 1988 Determination of the absolute magnetic moment direction in Cr_2O_3 using generalized polarization analysis *J. Appl. Phys.* **63** 3606–8
[16] Ye M and Vanderbilt D 2014 Dynamical magnetic charges and linear magnetoelectricity *Phys. Rev.* B **89** 064301
[17] Bousquet E, Spaldin N A and Delaney K T 2011 Unexpectedly large electronic contribution to linear magnetoelectricity *Phys. Rev. Lett.* **106** 107202

[18] Gonze X *et al* 2020 The Abinit project: impact, environment and recent developments *Comput. Phys. Commun.* **248** 107042

[19] Romero A H *et al* 2020 ABINIT: overview and focus on selected capabilities *J. Chem. Phys.* **152** 124102

[20] 2020 The ELK code: an all-electron full-potential linearised augmented-plane wave (LAPW) code (available at: https://elk.sourceforge.io/)

[21] Giannozzi P *et al* 2009 QUANTUM ESPRESSO: a modular and open-source software project for quantum simulations of materials *J. Phys.: Condens. Matter* **21** 395502

[22] Giannozzi P *et al* 2017 Advanced capabilities for materials modelling with Quantum ESPRESSO *J. Phys.: Condens. Matter* **29** 465901

[23] Kresse G and Furthmüller J 1996 Efficiency of *ab-initio* total energy calculations for metals and semiconductors using a plane-wave basis set *Comput. Mater. Sci.* **6** 15–50

[24] Kresse G and Furthmüller J 1996 Efficient iterative schemes for *ab initio* total-energy calculations using a plane-wave basis set *Phys. Rev. B* **54** 11169–86

[25] Blöchl P E 1994 Projector augmented-wave method *Phys. Rev. B* **50** 17953–79

[26] Delaney K T 2023 private communication

[27] The relevant input files and data of our *ab initio* calculations are openly available on the Materials Cloud Archive at https://archive.materialscloud.org/record/2023.171

[28] Lelièvre-Berna E, Brown P J, Tasset F, Kakurai K, Takeda M and Regnault L P 2007 Precision manipulation of the neutron polarisation vector *Physica B* **397** 120–4

[29] Tasset F, Brown P J, Lelièvre-Berna E, Roberts T W, Pujol S, Allibon J and Bourgeat-Lami E 1999 Spherical neutron polarimetry with Cryopad-II *Physica B* **267-268** 69–74

[30] Lelièvre-Berna E *et al* 2005 Advances in spherical neutron polarimetry with Cryopad *Physica B* **356** 131–5

[31] Qureshi N 2019 *Mag2Pol*: a program for the analysis of spherical neutron polarimetry, flipping ratio and integrated intensity data *J. Appl. Crystallogr.* **52** 175–85

[32] He X, Wang Y, Wu N, Caruso A N, Vescovo E, Belashchenko K D, Dowben P A and Binek C 2010 Robust isothermal electric control of exchange bias at room temperature *Nat. Mater.* **9** 579–85

[33] Borisov P, Ashida T, Nozaki T, Sahashi M and Lederman D 2016 Magnetoelectric properties of 500-nm Cr_2O_3 films *Phys. Rev. B* **93** 174415

[34] Weber S F and Spaldin N A 2023 Characterizing and overcoming surface paramagnetism in magnetoelectric antiferromagnets *Phys. Rev. Lett.* **130** 146701

[35] Perdew J A and Zunger A 1981 Self-interaction correction to density-functional approximations for many-electron systems *Phys. Rev. B* **23** 5048–79

[36] Liechtenstein A I, Anisimov V I and Zaanen J 1995 Density-functional theory and strong interactions: orbital ordering in Mott–Hubbard insulators *Phys. Rev. B* **52** R5467

[37] Shi S, Wysocki A L and Belashchenko K D 2009 Magnetism of chromia from first-principles calculations *Phys. Rev. B* **79** 104404

[38] Mu S, Wysocki A L and Belashchenko K D 2014 First-principles microscopic model of exchange-driven magnetoelectric response with application to Cr_2O_3 *Phys. Rev. B* **89** 174413

[39] Monkhorst H J and Pack J D 1976 Special points for Brillouin-zone integrations *Phys. Rev. B* **13** 5188–92

[40] Togo A and Tanaka I 2015 First principles phonon calculations in materials science *Scr. Mater.* **108** 1–5

[41] Togo A 2023 First-principles phonon calculations with phonopy and phono3py *J. Phys. Soc. Japan* **92** 012001

[42] Hill A H, Harrison A, Dickinson C, Zhou W and Kockelmann W 2010 Crystallographic and magnetic studies of mesoporous eskolaite, Cr_2O_3 *Microporous Mesoporous Mater.* **130** 280–6

[43] `thermo_pw` is an extension of the Quantum ESPRESSO (QE) package which provides an alternative organization of the QE workflow for the most common tasks. For more information see https://dalcorso.github.io/thermo_pw/

[44] Perdew J P, Burke K and Ernzerhof M 1996 Generalized gradient approximation made simple *Phys. Rev. Lett.* **77** 3865–8

[45] Vanderbilt D 1990 Soft self-consistent pseudopotentials in a generalized eigenvalue formalism *Phys. Rev. B* **41** 7892

[46] Dal Corso A 2014 Pseudopotentials periodic table: from H to Pu *Comput. Mater. Sci.* **95** 337

[47] See https://dalcorso.github.io/pslibrary/

[48] Baroni S, de Gironcoli S, Dal Corso A and Giannozzi P 2001 Phonons and related crystal properties from density-functional perturbation theory *Rev. Mod. Phys.* **73** 515–62

[49] Van Setten M J, Giantomassi M, Bousquet E, Verstraete M J, Hamann D R, Gonze X and Rignanese G-M 2018 The pseudodojo: training and grading a 85 element optimized norm-conserving pseudopotential table *Comput. Phys. Commun.* **226** 39